50 years of Geldart classification

Powder Technology 428 (2023) 118861

Contents lists available at ScienceDirect

Powder Technology

journal homepage: www.journals.elsevier.com/powder-technology

50 years of Geldart classification

Ray Cocco [a], Jia Wei Chew [b,*]

[a] Particles In Motion, LLC, Elmhurst, IL 61026, USA
[b] Chemical Engineering, Chalmers University of Technology, 412 96 Gothenburg, Sweden

HIGHLIGHTS

- Commemorate 50-years of Geldart classification by reviewing the four Geldart Groups.
- Compare Geldart classification with other such classifications.
- Provide perspectives on why the Geldart classification is so universal.
- Highlight precautions that need to be considered when using this classification.

GRAPHICAL ABSTRACT

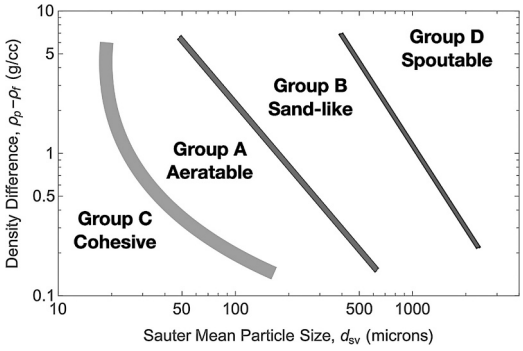

ARTICLE INFO

Keywords:
Geldart group
Gas-solid fluidization
Pressure drop
Minimum fluidization velocity
Bubbles

ABSTRACT

The Geldart classification reported in 1973 is widely acknowledged as one of the seminal papers on fluidization. Today, it remains the most used classification for particle fluidization. This is a simple comparison of the differential between particle and air densities versus Sauter-mean diameter, which successfully demarcates all particles into four distinctly different fluidization behaviors. To commemorate the 50th anniversary of this classification, an overview of the fluidization characteristics of the four Geldart groups is presented along with other such classifications, providing perspectives on why the Geldart classification is so universal. Some of the precautions that need to be considered when using this classification are also highlighted. This study is a tribute to the Geldart classification and is expected to be valuable as a summary of the advancements in the understanding of the Geldart groups to date.

1. Introduction

In 1972, an absurd paper was submitted to Powder Technology. It was accepted and published in 1973 [1]. The path to publication was not easy, and the author had to navigate through some rejections and revisions [2]. Today, it is one of the most referenced papers and used tools in fluidized beds and fluid-particle systems. Of course, this is the paper entitled "Types of Gas Fluidization" by Derek Geldart [1].

The fact that this paper had challenges may sound surprising today, but back in 1973, it was not wholly unfounded. Geldart's paper proposed that the fluidization behavior can be determined from the density difference and particle size. It seems back then to be an

* Corresponding author.
E-mail address: jia.chew@chalmers.se (J.W. Chew).

https://doi.org/10.1016/j.powtec.2023.118861
Received 13 May 2023; Received in revised form 25 July 2023; Accepted 1 August 2023
Available online 2 August 2023

oversimplification, if even true at all. Fifty years later, this paper and the research it is based on have thrived through the test of time, as shown in Fig. 1. Indeed, this paper has been cited almost 3000 times, and the number of citations continues to increase. For those involved in scaling up fluidized and circulating fluidized beds, it is Step 1 for any design calculation or optimization strategy.

Geldart's publication is based on a collection of fluidization data from different authors, the results of which are shown in Fig. 2. Empirical observations based on the density difference (i.e., $\rho_p - \rho_f$, where ρ_p is particle density and ρ_f is fluid density) and the particle size (specifically, Sauter-mean particle diameter, d_{sv}) show that the fluidization behavior can be classified into four distinct groups defined as A, B, C, and D. Particles in Group A exhibit dense phase expansion after minimum fluidization and before the onset of bubbles. Group B particles form bubbles at the onset of minimum fluidization. Group C particles are the smallest in size and, thereby are most cohesive in behavior. This group is the hardest to fluidize. The Group D particles are the largest and tend to form stable spouts such as those indicative of spouting fluidized beds. As long as fluidization continues to be industrially relevant, which is clearly the case as evident in newer applications like chemical looping, plastic pyrolysis, methane pyrolysis, etc., the prominent role of the Geldart classification will persist.

The demarcation between the fluidization behavior of each group was based on observations or concepts. For instance, the division between Groups C and A is based on empirical data. The division between Groups A and B is based on proportional relationships for estimating the minimum bubbling velocity and the criteria that the ratio of the minimum fluidization to superficial gas velocity is much >1. The result is that the density difference times the particle size, in microns, needs to be <225. Interestingly, this demarcation is close to that proposed earlier by Oltrogge [9]. The separation of Groups B and D is based on the bubble rise velocities study of Pigford and Baron [13] to generate a division line based on having the density difference multiplied by the square of the particle size being <106.

Remarkably, such demarcations provide an excellent first guess of the fluidization behavior. Such simplicity is unexpected, given the complex and multiscale hydrodynamics of fluidized beds. Here we describe the key characteristics of each Geldart group, discuss other such classifications, and highlight some precautions when using the Geldart chart.

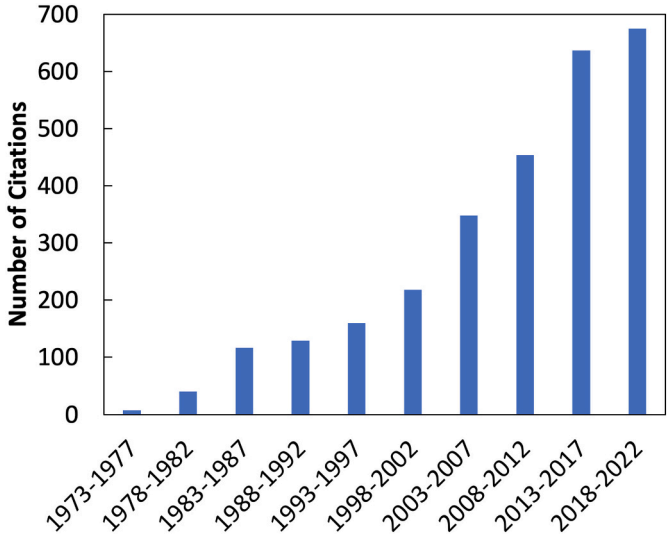

Fig. 1. 2785 documents have cited Geldart [1] through 2022 per Scopus. Retrieved on May 5, 2023.

2. Fluidization characteristics of each Geldart group

Regardless of the Geldart group, the minimum fluidization velocity can be measured from a pressure drop versus gas velocity curve. This method is illustrated in Fig. 3 and is based on ASTM D7742 [14]. Pressure drop monotonically increases with increasing velocity up to the point of fluidization. At this point, the superficial gas velocity is known as the minimum fluidization velocity (u_{mf}). At higher superficial gas velocities, the curve dips and then levels off to a value whereby the pressure drop across the bed corresponds to the weight of the bed divided by the cross-sectional area. This intersection of this slight dip and the plateaued pressure drop indicates the point of bubble formation (u_{mb}), which may or may not coincide with u_{mf}. However, this is a subtle feature, and precise determination of u_{mb} using the pressure drop versus gas velocity curve is often limited. Fortunately, the bed height can be used for such a determination, as shown in Fig. 4. While the pressure drop versus superficial gas velocity provides the u_{mf} value (Fig. 3) [14], the bed height versus the superficial gas velocity reveals the u_{mb} value (Fig. 4). The fluidized bed height is maximum just before the onset of bubbles. The bubbles bypass some of the gas in the emulsion, which makes the bed become slightly collapsed.

Once fluidized, the distinction in the fluidization behavior becomes apparent, as shown in Fig. 5, and is at the heart of Geldart's classification. The smallest Group C particles do not fluidize as they are too cohesive. Group A and the larger Group B particles have good fluidization characteristics, but the fluidization behaviors differ. The largest particles, Group D, tend not to be fully fluidized but exhibit a spouting behavior.

A simpler version of Fig. 2 has been presented, as depicted in Fig. 6. Despite its simplicity, it is remarkable how these differences align with the four groups for most particulate systems <2000 μm. Remarkable enough that it is worth discussing the defining characteristics beyond what is shown in Fig. 6.

2.1. Geldart Group C

Geldart Group C particles are the smallest particles in Fig. 2, specifically particles with a particle density of 1200 kg/m^3 having a particle size of 45 μm or smaller. Sometimes these particles are referred to as fines. Group C particles are defined as cohesive, which is attributable to interparticle forces such as van der Waals, electrostatics, or monolayer wetting (i.e., liquid bridging) [15]. What results is a poorly fluidized bed prone to channeling. Most of the fluidizing gas does not make it into the particle bed but bypasses it.

Fig. 3 illustrates the difficulty of fluidizing Geldart Group C material. Using a typical cylindrical column with good gas distribution, poor fluidization results, as indicated by the pressure drop profile after minimum fluidization has been achieved. Ideally, this part of the curve should be relatively flat and the pressure drop correspond to the force needed to suspend all the particles. What results is that the gas is mostly bypassing the bed through transient channels. The fluidization curve in Fig. 3 is a good test for determining if cohesive forces are an issue. The first indication is the less-than-stable pressure drop profile after minimum fluidization has been achieved. The second indication is the average pressure drop when the bed is fully fluidized, which should approximate the weight of the bed divided by the cross-sectional area of the column. In Fig. 3, this fell short by 32%.

To fluidize Group C particles, the gas distribution needs to be different than what is typically used for the other classifications. Rahman [16] found that fluidization improved significantly by adding an oscillating or pulse flow on top of a base flow for gas distribution. Pfeffer et al. [17] and Quevedo et al. [18] found that adding micro-jets into the bed significantly improved the fluidization quality. Good fluidization was found for even nanoparticles using micro-jet distributors. The resulting fluidization was smooth, with significant bed expansions compared to that in a traditional fluidized bed [19,20]. Trogadas et al.

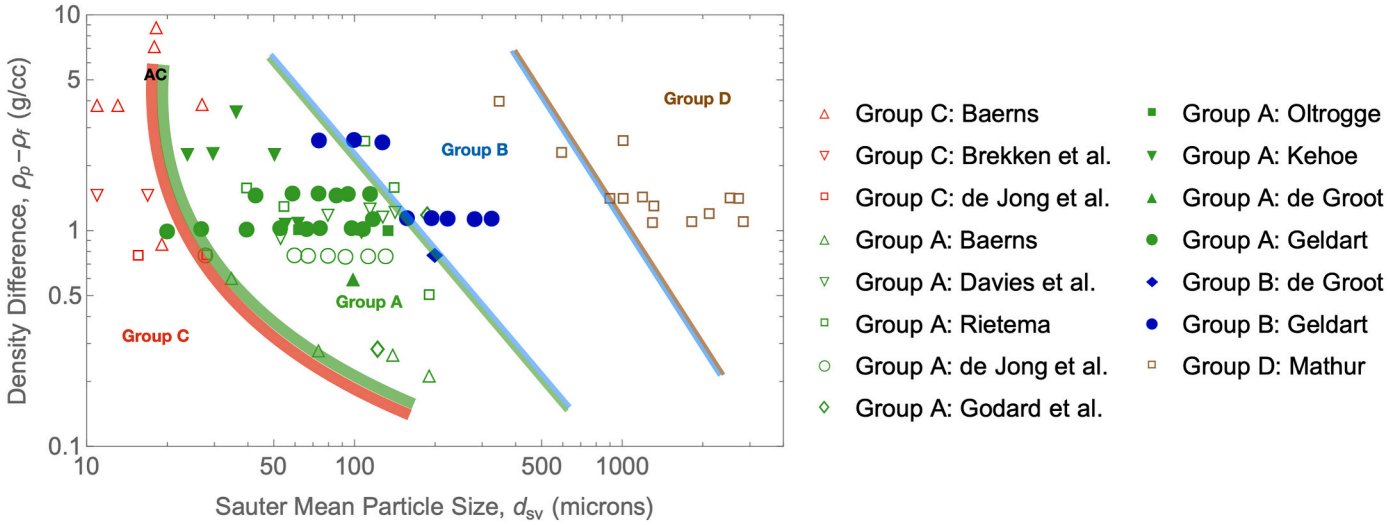

Fig. 2. Geldart classification of fluidization behavior. Modified and re-used with permission from Geldart [1]. The embedded studies are listed here for easy reference: Baerns [3], Brekken et al. [4], de Jong et al. [5], Davies et al. [6], Rietema [7], Godard et al. [8], Oltrogge [9], Kehoe et al. [10], de Groot [7], Geldart [11], and Mathur [12].

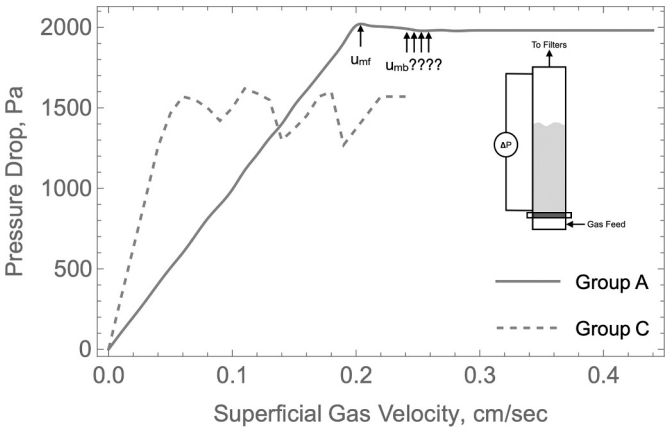

Fig. 3. Pressure drop versus increasing superficial gas velocity in a column of 14 kg of Group A or C particles. The column diameter is 0.3 m.

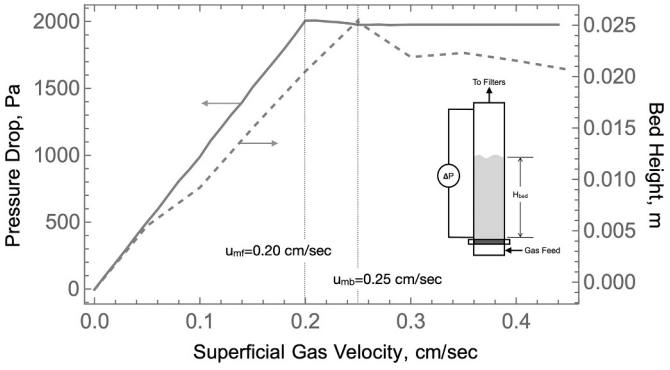

Fig. 4. Pressure drop and bed height measurements versus increasing superficial gas velocity in a column of 14 kg of Group A particles. The column diameter is 0.3 m.

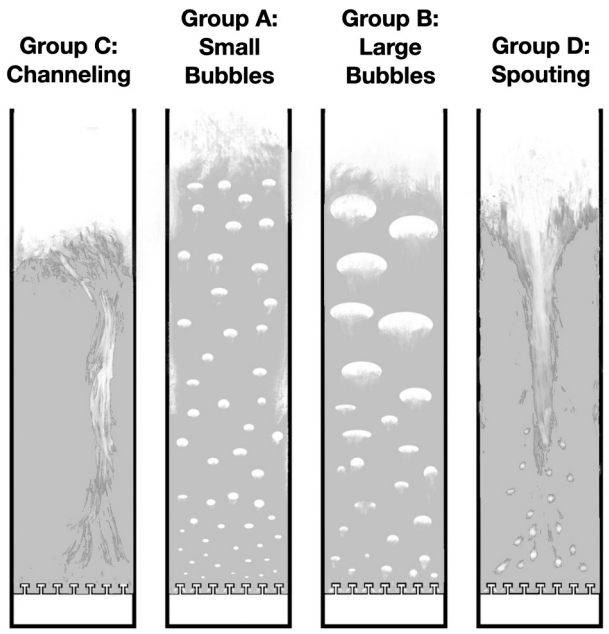

Fig. 5. Illustration of the fluidization behavior of each Geldart group.

[21] expanded on this concept by using a multi-layered fractal distributor design that resembles the hierarchical structure found in lungs.

2.2. Geldart Group A

Group A has been the key driver for the extensive research on fluidized beds. These particles are the most common to fluidize for several reasons. They are arguably the easiest to produce using a commercial scale spray drier since particle sizes tend to range from 45 to 150 μm with particle densities of 800 to 2000 kg/m^3. Also, when fluidized, these Group A particles have relatively high heat and mass transfer, making them ideal for fast, exothermic reactions. Indeed, Group A particles are at the heart of breakthrough fluidized bed technologies, including acrylonitrile, polyolefin (Unipol), oxychlorination, and catalytic oxidization [22].

The key fluidization characteristics distinguishing Geldart Group A

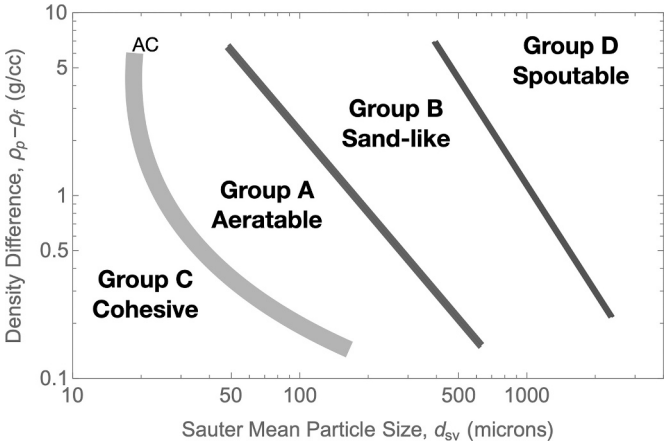

Fig. 6. Interpretation of Geldart groups.

particles from the other groups are bubble hydrodynamics and permeability. For Group A particles, the bubble size tends to be small, on the order of 5 cm. In particular, the bubbles do not form at the onset of fluidization, defined as the minimum fluidization velocity (u_{mf}). Higher superficial gas velocities are needed for bubbles to form, the threshold of which is referred to as the minimum bubbling velocity (u_{mb}). The region between u_{mf} and u_{mb} is called homogenous or smooth fluidization [23]. Groups B and D do not exhibit this behavior, as the minimum bubbling velocity is the same value as the minimum fluidization velocity (i.e., $u_{mb} = u_{mf}$).

Speculations revolving around the physical origins of homogeneous fluidization of Group A particles remain incompletely resolved, with some attributions to hydrodynamics related to fluid-solid interactions while others to solid-solid interactions. Regarding hydrodynamics, Garg and Pritchett [24] were able to simulate homogeneous fluidization behavior by adding any force proportional to the spatial gradient of particle concentration to the particle momentum equation. Foscolo and Gibilaro [25] formulated a hydrodynamic criterion for the onset of bubbling based on the relative magnitudes of voidage propagation and elastic wave velocities, while Verloop and Heertjes [26] presented another such criterion based on the elasticity modulus calculated from a drag force – interparticle distance relationship. Menon and Durian [27] found particle motions and fluctuations to be minimal in homogeneous fluidization, while Cody et al. [28] related average granular temperature to differences in fluidization behaviors between Groups A and B. As for interparticle forces, Rietema [29] demonstrated that cohesion and friction can result in an effective elastic modulus that maintains a stable bed, while Tsinontides and Jackson further provided evidence that yield stresses from solid-solid contacts are responsible for the stabilization [30]. Foscolo and Gibilaro [25] and Pandit et al. [31] had similar arguments. Further evidence was shown by Valverde et al. [32,33], in which the addition of fumed silica to the bed caused the bed to display homogenous behavior over a wider range of velocities due to the reduced cohesion. If interparticle forces are at play for homogeneous fluidization, particle clustering also plays a role. Royer et al. [34] showed that adding fumed silica to larger particles reduces the cohesive forces, leading to diminished clustering caused by increased surface roughness increasing the translational momentum [35,36]. A recent study demonstrated the homogeneous fluidization behavior to be due to both hydrodynamics and solid-solid interactions [37].

Bubble behavior is different for Group A particles compared to Group B or D particles. Generally, as shown in Fig. 7, bubbles start small at the bottom of the bed and grow as they rise through the bed. w et al. [38], Werther [39], and Cai et al. [40] have empirical models to estimate the bubble growth in a fluidized bed. Werther's correlation requires an initial bubble size that can be captured from the work of Kobayashi et al. [41] and Miwa et al. [42]. Regardless of the bubble growth model, the

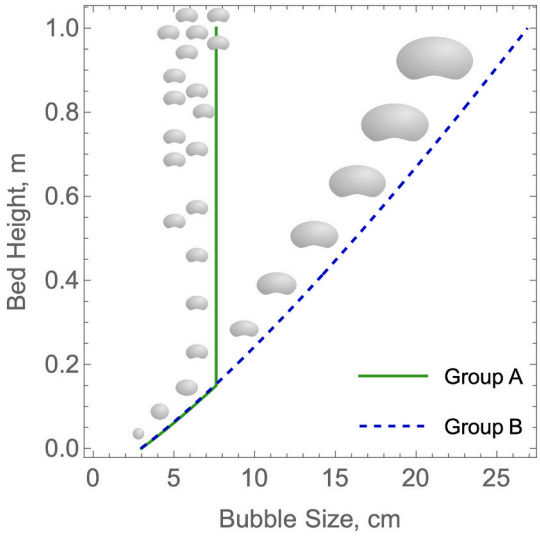

Fig. 7. Bubble growth versus bed height for Geldart Group A and B particles using Darton et al. [38] for 70 and 200 μm particles with a particle density of 1.5 g/cm^3 and superficial gas velocity of 0.5 m/s.

maximum or equilibrium bubble size needs to be considered for Group A particles. Geldart [43] estimated this based on the terminal velocity. Fig. 7 illustrates this type of bubble growth in a fluidized bed, specifically that the bubbles grow to their maximum bubble size with splitting and coalescence in equilibrium. In short, Group A particles can only support a maximum bubble size before it becomes unstable and breaks up or resist any additional gas. The maximum bubble size is due to the lower bed permeability of Group A compared to the larger particles of Group B or D. Smaller particles have a higher surface-to-volume ratio than larger particles, and the higher particle surface area contributes to a greater drag force. This limitation makes it more difficult for the gas in the bubble to exchange with the gas in the emulsion. As a result, a more stable configuration for the fluidization of Group A particles is more small bubbles and less large bubbles, as depicted in Fig. 7.

Such behavior can also be seen by adding fines ($d_p < 44$ μm; Group C) to a fluidized bed of Group A particles. The bed expands, the fluidization becomes more stable, and bubbles get smaller [44,45]. The presence of fines holds more gas or fluid due to its higher surface area and the resulting drag force. These fines are more mobile in the bed and can move more gas into the emulsion phase. As a result, the bed expands to account for the increase in gas volume in the bed, which means there is less gas for the bubbles [46].

Notably, a bed of Group A particles devoid of fines has been shown to exhibit the opposite effect. Bubbles are larger and the fluidized bed is more chaotic. An extreme case of this would be gas bypassing. Gas bypassing results from one or more streams of very fast-moving bubbles rising upwards in the bed. Since most of the gas is in the form of these streams, which represents the path of least resistance, the remaining portion of the bed is nearly defluidized [47]. It is a phenomenon that occurs with Group A particles in deep or dense beds. The bed's low permeability combined with the higher pressure at the bottom of the bed due to the deep or dense bed results in instability. At this point, any trigger can form these stable but transient streams of fast-moving large bubbles. One of the solutions to mitigate gas bypassing is the addition of fines to the bed. According to Issangya et al. [47], increasing the bed fines content from 4 wt% to 8 wt% can expand the bed height from 1 m to 2 m, because adding fines allows more gas to be moved into the emulsion and thus mitigates the precursor for these gas streams [48].

Another distinguishing characteristic of Group A particles is the rate of defluidization when the fluidizing gas is shut [7]. This defluidization behavior is shown in Fig. 8 for Groups A and B particles. The rate of bed collapse or the rate at which the bed height comes to rest depends on the

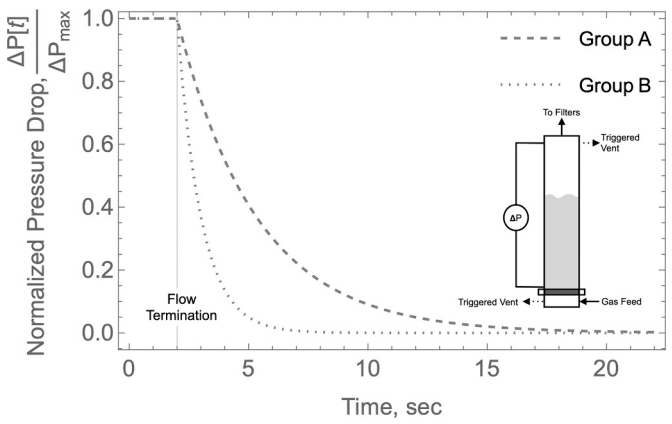

Fig. 8. Concept of collapsing fluidized bed curves for Geldart Group A and B particles whereby the gas flow is terminated along with venting of the freeboard and plenum. The column diameter is 0.3 m.

bed's permeability. For Group A particles, the rate of collapse is much longer than that of other groups. For Group B particles, because of the much higher gas permeability in the bed, defluidization is quick [49]. For example, as shown in Fig. 8, in a 0.3-m diameter column with a 0.5-m deep bed, Group A particles could take >15 s to defluidize, whereas Group B particles would be defluidized in <5 s. Geldart and Wong reported that the de-aeration times of Group A particles is most affected by particle density, followed by particle size, fines fraction, gas viscosity and gas density [49]. Simulation studies subsequently showed that solids modulus is the dominant factor affecting deaeration, and that two different hydrodynamic models, two different drag models and solids rheology have negligible effect [50]. More studies are needed to fully understand the physical basis.

It needs to be noted that when using Fig. 2 to discern if a particle behaves according to Group A or C behavior, the Geldart Classification Chart provides less predictive accuracy. The broader boundary denotes A/C behavior, and if the particle falls in this region, it could behave like Group A or C [1]. Only experimental testing will reveal its actual fluidization behavior, which should probably be done under actual operating conditions [49,51,52]. However, even if the particles are characterized as Group C from testing, they could behave as a Group A particle at elevated temperatures [53] or with a higher viscosity gas [54]. The opposite may be true at higher pressures [55].

2.3. Geldart Group B

Geldart Group B particles have particle sizes ranging from 150 to 1000 μm, for the most part. Typically Group B particles do not exhibit significant cohesive behavior primarily due to their large size dominating the fluidization hydrodynamics (i.e., body forces dominate over surface forces). The fluidization of such particles is typically described as having much larger bubbles and much faster defluidization rates than Group A or C particles. Sand is a good representation of a Geldart Group B particle.

Arguably, the most interesting characteristic of Group B particles is the bubble growth. As shown in Fig. 7, bubbles in a fluidized bed of Group B particles continue to grow, with no equilibrium bubble size being reported. In tall commercial units, bubbles can grow to the order of meters [44]. Such large bubbles could be an issue with commercial applications of Group B particles. If the bubble size increases enough, slugging could result [23]. The vibrational stresses on such units could be concerning.

With the permeability of Group B particles being significantly higher than for Group A or C particles, the fluidization behavior is notably different. The lower drag and the relative absence of cohesive forces drive this lower permeability. The gas can more easily flow around the particles; thus, more gas is needed to suspend the particles. As a result, bubble formation occurs at the point of fluidization (i.e., $u_{mf} = u_{mb}$), and the fluidized bed height tends to be lower than that for Group A particles or a well-fluidized bed of Group C particles. Indeed, one discerning test for characterizing a particle as Group B is measuring the agreement of the minimum fluidization and minimum bubbling velocities (Fig. 4).

The commercial applications involving Group B particles are less than that of Group A ones. The larger bubbles contribute to a lower mass transfer which for heterogeneous processes could be limiting. The higher superficial gas velocities needed reduce the gas residence time, which can also be a limiting factor. Another issue is that the making of Group B particles is more challenging than with Group A. These particles tend to be harder to spray dry in commercial units, a common method for making Group A particles, and it is expensive to mill Group B particles from extrudes.

However, Group B particles have seen prominent applications in gasification and pyrolysis. Natural Group B materials such as quartz or silica sand can provide the mixing and thermal stability needed for such reactions in a fluidized bed. Since the reactions are homogeneous, bubble size is less of an issue for these applications.

2.4. Geldart Group D

Group D particles tend to have particle sizes larger than 1000 μm and are characterized as spoutable. Very dense particles can also be characterized as Group D, even with particle sizes smaller than 1000 μm (e.g., metal particles). Bed densities tend to be higher for Group D particles, which limits mixing. Like Group B particles, Group D particles tend to have large bubbles. Geldart [1] noted that all but the largest bubbles tend to rise slower than the gas in the emulsion. Unlike Group A or B particles that form fast clouded bubbles (i.e., bubble rise velocity is higher than interstitial gas velocity, and gas circulates between bubble and cloud), Group D particles tend to form slow cloudless bubbles (i.e., interstitial gas velocity is higher than bubble rise velocity, and emulsion phase gas flows through the bubble phase from bottom to top with negligible circulation) [56].

The gas flow through a bed of Group D particles must be high to fluidize the bed. As a result, Group D applications tend to be limited to particle processing, not gas processing. Gas residence times are too short for most practical applications whereby the gas effluent would be the product. Also, unlike Group B particles, increasing the gas velocity through a fluidized bed can form a jet or spout, as shown in Fig. 5 [57,58]. Such behavior is exploited with particle coating/treatment and granulation operations. The spouting jet can be controlled and stabilized using a conical fluidized bed and/or draft plate [59,60].

3. Geldart Classification versus other classifications

The inevitable question is, in view of the lack of in-depth mathematical analysis and basing just on bubbling behavior observations, why did the Geldart chart persist to be the dominant chart for classifying particles into Groups representing different fluidization behaviors? A straightforward answer is the sheer simplicity to use it. To further address this, it is necessary to review other available classifications. A commonality in these alternatives appears to be on additionally accounting for the gas phase, since the Geldart classification essentially ignores gas phase properties. More specifically, even though ρ_f is accounted for on the *y*-axis (Fig. 2), the term $\rho_p - \rho_f$ negates any effect of ρ_f as ρ_p is typically three orders of magnitude larger than ρ_f for fluidization by gas.

In 1984, Rietema [54] presented a dimensionless version of the Geldart chart to additionally factor in cohesion, gas viscosity and gravitational acceleration. As shown in Fig. 9a, the *x*-axis accounts for a cohesion factor *C* (whereby a characteristic value for *C* was given as 4 N/m^2 for particle diameter (d_p) = 100 μm, fluid viscosity (μ) = 2 × 10^{-5}

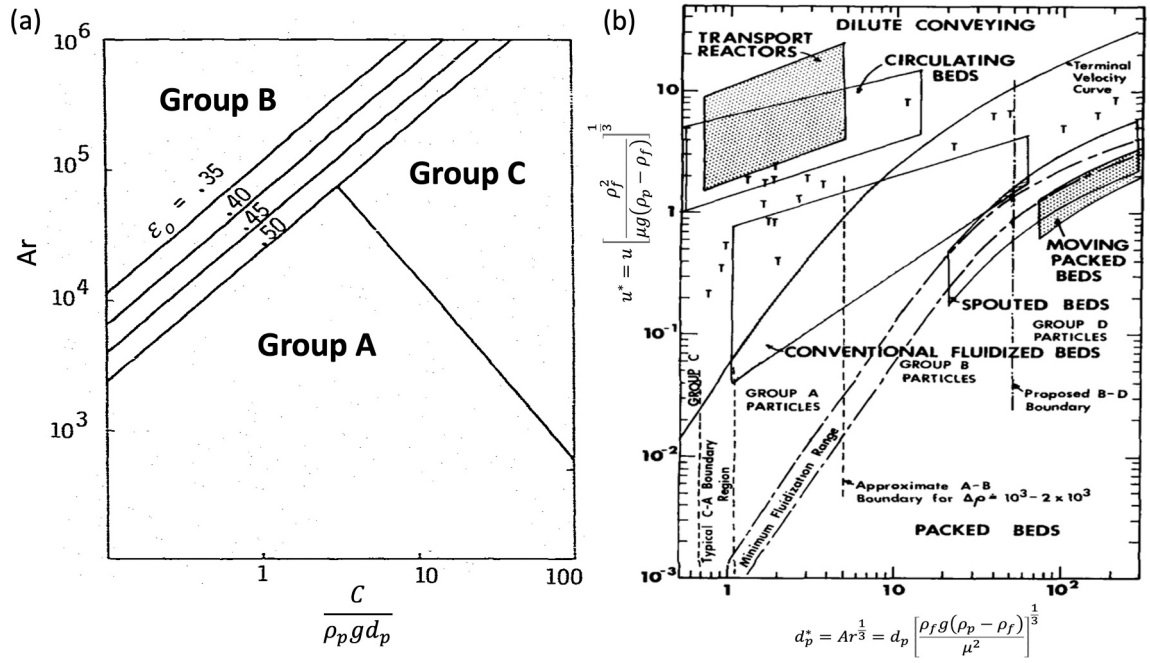

Fig. 9. (a) Rietema's dimensionless presentation of the Geldart classification [54], reproduced with permission from Elsevier; and (b) Grace's regime map with new boundaries for the Geldart groups superimposed [61], reproduced with permission from Wiley.

Ns/m^2 and superficial gas velocity (u) > 0.1 m/s), while the y-axis is Archimedes number (Ar; ratio of gravitational force to viscous force):

$$\mathrm{Ar} = \frac{g d_p^3 \rho_f (\rho_p - \rho_f)}{\mu^2}$$

where g is gravitational acceleration, d_p is particle diameter, and μ is fluid viscosity. The A-B boundary was defined based the premise that homogeneous expansion is possible only when the elastic compensating force exceeds the continuity wave force and is dependent on packed bed porosity (ε_o). As for the A-C boundary, the negative slope reflects the dominance of cohesion as well as the corresponding impact of gas viscosity; however, it was indicated that the exact position and slope need further investigation.

In 1986, Grace [61] presented a fluidization regime map superimposed with new boundaries for the Geldart groups (Fig. 9b). The boundaries for Groups A-B and B-D were modified to account for gases other than air as well as for non-ambient temperarure and pressure, and also to include studies reported since the Geldart chart was published. Similar to Rietema [54], the axes are dimensionless. While the x-axis is dimensionless particle diameter (d_p^*), the y-axis is dimensionless superficial velocity (u^*):

$$d_p^* = Ar^{\frac{1}{3}} = d_p\left[\frac{\rho_f g(\rho_p - \rho_f)}{\mu^2}\right]^{\frac{1}{3}}$$

$$u^* = u\left[\frac{\rho_f^2}{\mu g(\rho_p - \rho_f)}\right]^{\frac{1}{3}}$$

Based on classifying data into Groups A if $u_{mb} > 1.2u_{mf}$ and Group B if $u_{mb} < 1.1u_{mf}$, the new A-B boundary established is such that Group A and B particles remain in the same classification in the same gas at different temperatures and pressures. As for the new B-D boundary, the physical bases are the distinction between fast cloudy bubbles for Group B and slow cloudless bubbles for Group D, and the ability to spout for Group D. It was noted that the boundary does not account for changes of gas physical properties since such data were not available.

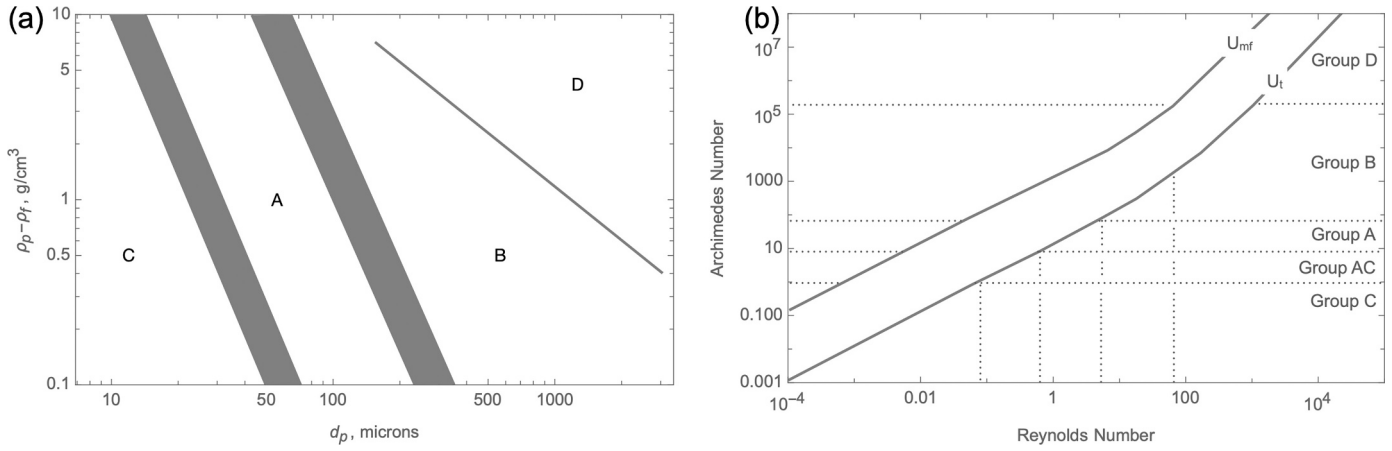

Fig. 10. (a) Geldart classification with boundaries per Molerus [62], reproduced with permission from Elsevier; (b) Goossen's classification on a log-log plot of Ar versus Re [63], reproduced with permission from Elsevier.

In 1993, Molerus [62] showed that consideration of the relative magnitude of the inter-particle adhesion forces with respect to the drag forces results in a classification similar to that of Geldart [1], as illustrated in Fig. 10a. Based on the limiting isostatic stress in a random-packed bed, the average tensile force per particle was defined by:

$$F_T = \frac{\pi}{6}\frac{F_H}{\varepsilon}$$

where F_H is the adhesion force per particle contact (e.g., 7.71×10^{-7} N for polypropylene, 8.76×10^{-8} N for glass beads) and ε is bed porosity. In particular, F_H is affected by the surface geometry of the particles in contact, nature of the inter-particle interaction force and the hardness of the particles. To express drag force, the Euler number for fluidization, which is the ratio of drag per particle to fluid dynamic pressure, was used:

$$\mathrm{Eu_{Fl}} = \frac{4}{3}\frac{\rho_p - \rho_f}{\rho_f}\frac{d_p g}{u^2}\varepsilon^2$$

and u is superficial gas velocity. The A-C boundary is characterized by the non-dimensional group of maximum drag force normalized by average tensile force, based on the premise that the predominance of inter-particle cohesion forces of Group C particles suppresses free particle motion. The broader boundary is underlain by the hardness of the particles, with the left-hand limit for harder particles and the right-hand limit for stronger adhesion forces associated with less hard particle surfaces. The same argument applies to the A-B boundary, based on adhesion forces being negligible relative to drag forces for Group B. As for the B-D boundary, the limit was based on the tendency to spout when the dynamic pressure of the fluid exceeds a critical value at the onset of fluidization.

In 1998, Goossens [63] proposed a classification based on Ergun's popular summation of laminar and turbulent constituents in packed-bed flows [64], and it was indicated to be generally valid for any temperature and pressure. Specifically, based on the relative dominance of laminar and turbulent phenomena, a classification on a log-log plot of Ar versus Re was reported, as shown in Fig. 10b. The Reynolds number (*Re*; ratio of inertial force to viscous force) is calculated by:

$$Re = \frac{\rho_f d_p u}{\mu}$$

Four boundaries are set based on the relative dominance of laminar and turbulent effects: (1) the C-AC boundary is defined at the entrainment benchmark whereby the laminar effects are 1000 times that of the turbulent ones, giving $\mathrm{Ar_1} = 0.97$; (2) the Group A-B boundary is defined at the minimum fluidization benchmark and similarly at the critical laminar-to-turbulent ratio of 1000, giving $\mathrm{Ar_2} = 88.5$; (3) the Group B/D boundary is defined such that the laminar and turbulent effects are equal at the onset of fluidization, giving $\mathrm{Ar_3} = 176{,}900$; and (4) the Group AC-A boundary is defined based on considerations that at least 1% of the hydrodynamics is turbulent since local cohesion has to be overcome by fluid inertia forces, giving $\mathrm{Ar_4} = 9.8$.

Comparing the resulting classification with Geldart's in Fig. 11a indicates agreement on the boundaries except for the A-B one, which has been tied to different perspectives of the onset of bubbling. As for the comparison between the Goossen and Molerus classifications, Fig. 11b indicates better agreement between the former basis on the Archimedes number, and the latter experimental basis on bubbling and heat transfer phenomena. In brief, the Goossens boundaries representing Ar values of 0.97, 9.8, 88.5, and 176,900 divide the particles into five categories corresponding to Geldart Groups C, AC, A, B and D. This classification converges with the Geldart classification [1] for fluidizing with ambient air, which the latter was experimentally developed for.

The Geldart classification was developed using fluidization with ambient air, which brings into question the applicability for industrial operations that involve gases other than air, and are typically at high temperatures and pressures. The experimental results of Grace [61] and Oltrogge [9] suggest that the Group A-B boundary is more depressed than that initially proposed by Geldart [1]. Grace devised a new Ar-based A-B boundary for such data [61], which agrees with that of Geldart. Specifically, Ar, which represents the ratio of body forces to viscous forces, can better account for differences in the hydrodynamics due to changes in gas density and viscosity. Later on, Goossens [63] also proposed using Ar. Additionally, instead of merely density difference, normalized density difference (i.e., normalized with respect to the gas density) was noted to better reflect gas pressure effects. Correspondingly, the Group A-B boundary was described with the Archimedes number of 88.5, and the transition from homogeneous to bubbling fluidization or laminar to turbulent flow effects can be better captured [63]. Fig. 12 shows Yang's [19] re-evaluation of Fig. 2 in terms of the normalized density and the Archimedes number proposed by Goossen [63], along with the boundaries proposed by Grace [61] and Oltrogge [9]. The Group A-C boundary is more curved. The Group A-B boundary is less discrete, and there is no reason not to expect the B-D boundary to be as discrete either. Accounting for gas properties, the general consensus is that Group B particles tend to behave as Group A at high pressure, and even Group D fluidizes as Group A at sufficiently high pressure. More on this chart is discussed in the subsequent section on precautions needed when using the Geldart Chart for high-temperature and high-pressure systems fluidized with fluids other than air.

In 2023, a new classification was presented, serving as a testament to the continued interest in classifying particles into different fluidization

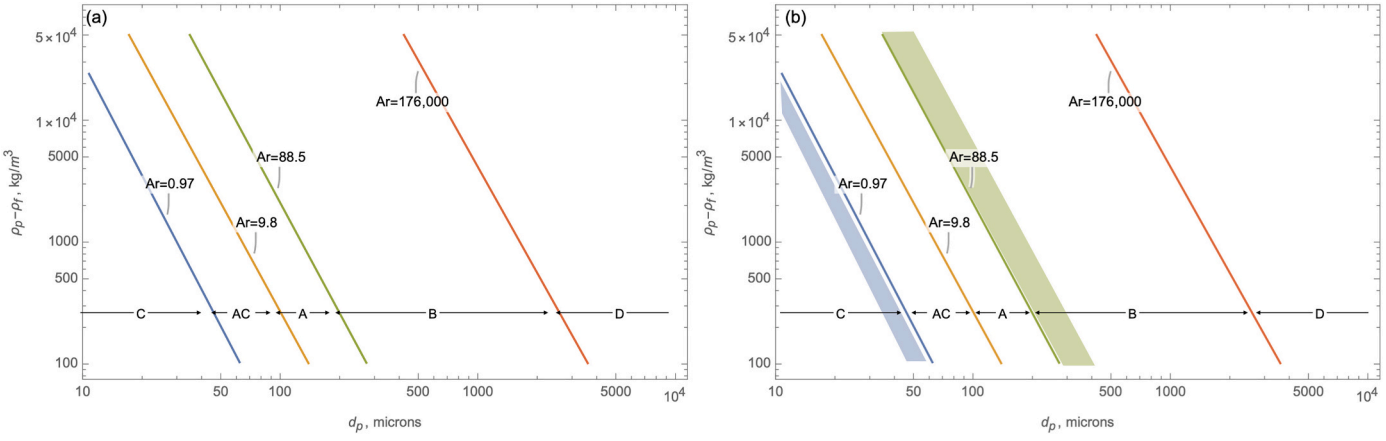

Fig. 11. Goossens classification [63], with (a) the Geldart classification embedded [1], and (b) the Molerus classification superimposed with broader demarcations [65]. Modified and re-used with permission from Elsevier.

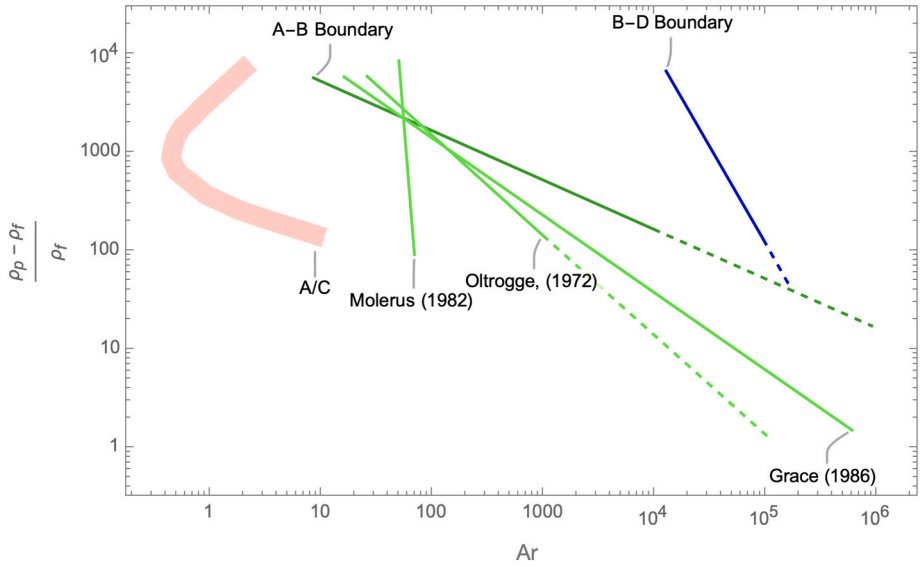

Fig. 12. Yang [19] classification, based on modifying Geldart's classification of particles and re-casting the axes as dimensionless density and Archimedes number. Dashed lines represent extrapolations. Modified and re-used with permission from Elsevier.

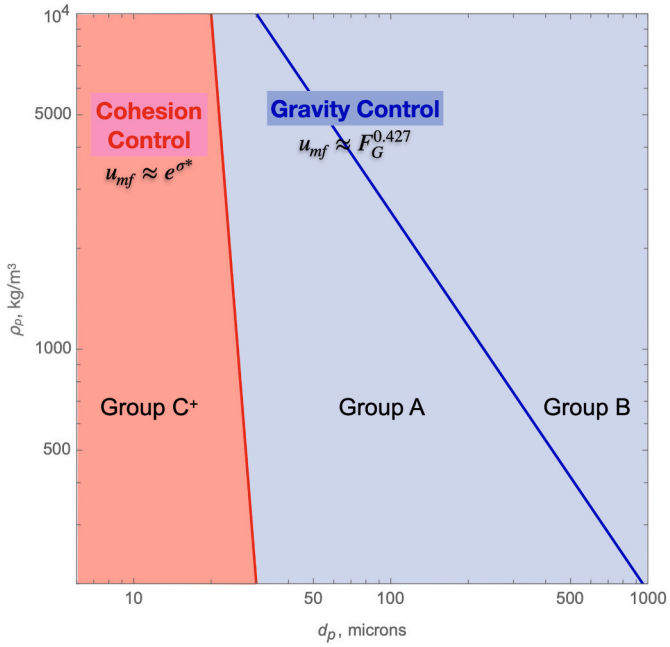

Fig. 13. Zhou et al. [20] classification with a new Group C$^+$. Modified and re-used with permission from Elsevier.

behaviors [20]. The relative influences of cohesion and gravity on minimum fluidization velocity (u_{mf}) result in the classification in Fig. 13. A new group (namely, Group C$^+$) was reported. Specifically, the original Group C particles were surface-modified to reduce cohesiveness and thus become fluidizable. This is reminiscent of the earlier studies on adding of fumed silica nanoparticles to mitigate cohesion [32–34]. The minimum fluidization velocity (u_{mf}) of the new Group C$^+$ was found to increase with a revised Archimedes number (Arσ^*) that factors in a cohesion index (σ^*; ratio of cohesion to gravitational forces):

$$\mathrm{Ar}\sigma^* = \frac{\sigma d_p^2 \rho_f \varepsilon}{\mu^2}$$

where

$$\sigma^* = \frac{F_\sigma}{F_G} = \frac{\sigma \varepsilon d_p^2}{d_p^3 \rho_p g} = \frac{\sigma \varepsilon}{d_p \rho_p g}$$

where σ is cohesion measured by the FT4 instrument with unit of Pa, F_σ is cohesive force, F_G is gravitational force. Fig. 13 thus modified the Geldart classification by adding (i) a new fluidizable Group C$^+$; and (ii) the different corresponding u_{mf} calculations based on the dominance of cohesive force for Group C$^+$ while gravitational force for Groups A and B:

$u_{mf} \approx e^{\sigma^*}$ for Group C$^+$

$u_{mf} \approx F_G^{0.427}$ for Groups A and B

4. Analogous to Geldart classification: pneumatic conveying

In 2005, Kalman et al. [66] classified particles into three different zones based on their pickup velocity (u_{pu}) in pneumatic conveying in both gas and liquid. Specifically, pickup velocity is defined as the critical velocity to move the particles at rest [67], which is important for predicting the velocities required for such applications. Fig. 14 depicts the three-zone model. For the *y*-axis, a modified Reynolds number was used to account for the effect of pipe diameter on u_{pu}. The relationship between the u_{pu} values in various pipe diameters and those in a pipe diameter of 50 mm was found to be:

$$\frac{u_{pu}}{u_{pu,50}} = 1.4 - 0.8e^{-\frac{D/D_{50}}{1.5}}$$

where D is pipe diameter and the subscript 50 refers to the reference pipe diameter of 50 mm. Accordingly, the modified Reynolds number was expressed as:

$$Re_p^* = \frac{\rho_f d_p u_{pu}}{\mu\left(1.4 - 0.8e^{-\frac{D/D_{50}}{1.5}}\right)}$$

Regarding the three zones, Zone I is for free-flowing sand-like materials, Zone II is for particles with non-negligible cohesive forces and lower permeability, while Zone III is for particles with significant cohesive forces and thus cannot be picked up individually. Clearly,

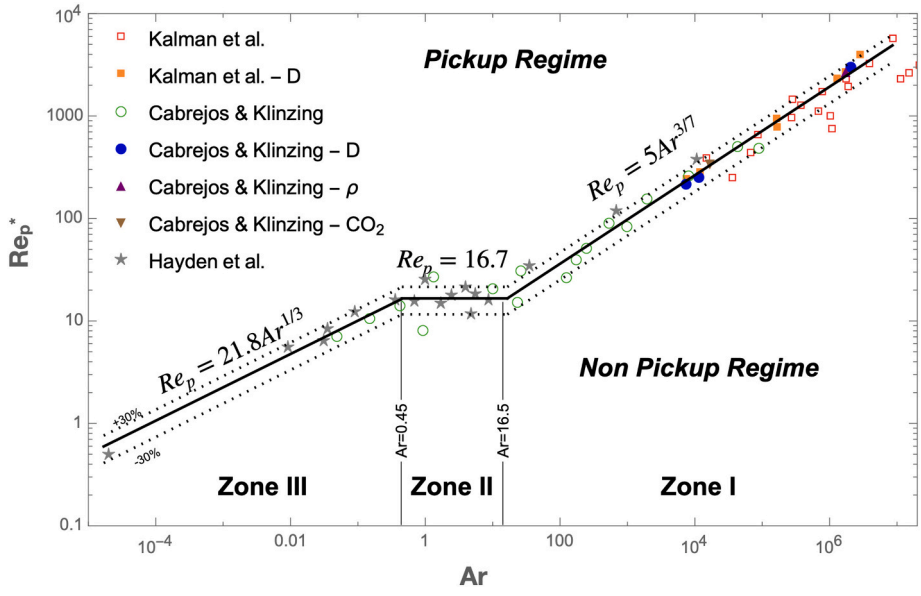

Fig. 14. Classification of particles for pneumatic conveying, where $Re_p^* = \frac{\rho_f d_p u_{pu}}{\mu\left(1.4-0.8e^{-\frac{D/D_{50}}{1.5}}\right)}$, where D is the pipe diameter used and D_{50} = 50 mm. Zones I, II and II correspond respectively to Geldart Groups B, A and C. Reproduced with permission from Kalman et al. [66]. The embedded studies are listed here for easier reference: Kalman et al. [66], Cabrejos and Klinzing [69–71], and Hayden et al. [72].

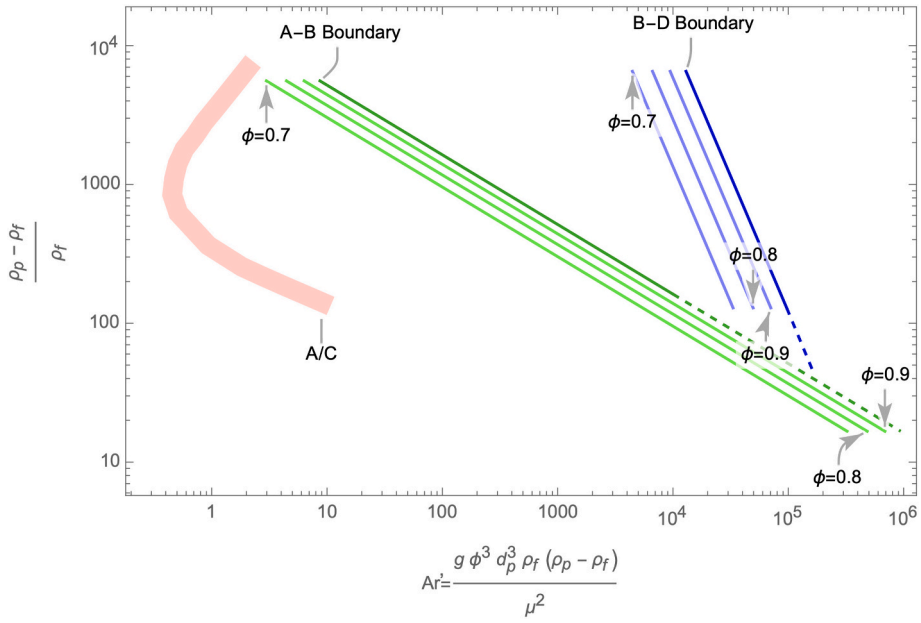

Fig. 15. Effect of particle sphericity on the modified Geldart classification of fluidization behavior.

Zones I, II and III correspond to Geldart Groups B, A and C. For nanoparticles, it was further found that, although nanoparticles belong in Zone III, they are described by the correlation for Zone I particles in pneumatic conveying due to agglomeration [68].

5. Precautions when using the Geldart Chart

Although the Geldart Classification chart in Fig. 2 is widely endorsed as the first step in designing or optimizing a fluidized bed operation, it has some limitations. Fig. 2 shows a broad boundary between Geldart Groups A and C particles, which are sometimes classified as Group A/C particles. Similarly, the distinctions between Groups A and B, and Groups B and D, are less clear at the boundaries. Indeed, many factors can impact the differentiation between Groups, such as temperature, pressure, sphericity, roughness, cohesion, and adsorbed species. So, some vigilance is warranted, as noted as follows.

5.1. Temperature and pressure

The Geldart classification was developed with ambient air, and thereby caution is necessary for industrial operations. Concern was noted by many [19,54,61], who proposed that the Geldart classification of particles does not apply at elevated temperature and pressure when using fluidizing gases other than air. Fluidization above room temperature applies to most fluidized bed unit operations besides dryers and heat treaters. The Geldart classification only depends on density

difference ($\rho_p - \rho_f$) and particle size. Yet, despite using the density differences, particle densities tend to be 1000 times higher than the gas density, which means the Geldart classification chart largely only considers the particle size and the particle density. Thus, Fig. 2, in principle, does not consider gas viscosity or gas density, which certainly impacts the particle drag force and the damping of such drag forces [73]. With temperature affecting both gas viscosity and density, and pressure affecting gas density, one would expect these classifications to be impacted.

The benefit of using Ar in Fig. 12 is that some of the temperature effects are captured. For example, a 125-μm particle with a particle density of 1800 kg/m^3 in propylene gas would be classified close to the A-B boundary in the original Geldart Chart (Fig. 2). In Fig. 12, this particle point would be classified as Group B at 25 °C, but Group A at 600 °C. Therefore, for classifications close to boundary lines, using the Archimedes number may be a better approach.

The system pressure also adds complexity to the interpretation of the Geldart classifications. At higher pressures, smaller or less dense Group B particles may exhibit Group A behavior, whereas at lower pressure, such behavior was observed to be clearly in line with the Group B classification [74]. Yet, according to Fig. 2, increasing the absolute pressure from 1 to 10 bar only changes the density differences by 1% for a 1200 kg/m^3 particle density. For the log-log plot in Fig. 2, there is no classification change at all. Notably, Liu et al. [75] reported that Group D particles fluidized with CO_2 at pressures higher than 4 MPa resulted in homogeneous bed expansion reminiscent of Group A particles below the minimum bubbling velocity.

5.2. Fines

The x-axis of the Geldart classification chart (Fig. 2) is surface-volume mean diameter. Many different definitions of the mean diameter are available; for the same particle size distribution, while the number-based mean gives a smaller value due to the greater emphasis on the finer particles, the volume-based one gives a larger value to emphasis on the coarser particles [76]. In practical applications, the surface-volume mean diameter is typically used due to the underlying physical association with the ratio of drag to gravitational forces. Past studies have shown the significant impact of fine particles on fluidization behavior. Pell noted that fluidization becomes more stable and bubbles get smaller [44]. Marnani et al. [77] reported that increasing the amount of Geldart Group C particles in a Geldart Group A bed leads to different fluidization behaviors, with notable differences including an increase in the hysteresis between fluidization and defluidization curves, the peak pressure drop occurring at a higher velocity, and a decrease in bed expansion. Issangya et al. [78] showed that the presence of more fines mitigated the gas bypassing behavior and thus allowed for the operation of taller Group A beds. Bareschino et al. [79] investigated the fluidization of pyroclastic particles, and found that fines promoted homogeneous fluidization, allowing for the operation of bubble-free fluidization over a wider range of superficial gas velocities. These studies collectively elucidate the important influence of fines, as well as the nature of the particle size distribution, on impacting fluidization behavior, which cautions the use of surface-volume diameters on the Geldart chart for predicting fluidization tendencies.

5.3. Inter-particle forces

Inter-particle forces such as van der Waals, Coulombic, and wetting forces may need to be considered for the classification of particles. While larger particles are less affected by such forces, past studies have shown them to be significant in some cases. Yehuda et al. [80] showed that adding moisture to Group D particles resulted in fluidization behavior indicative of Group A or even Group C particles due to van der Waals and liquid bridging forces. Seville and Clift [81] presented similar tendencies, specifically that wetted Group B particles behave like Groups A and C.

Electrostatics is well-acknowledged to affect bed hydrodynamics [82]. Mehrani et al. [83] found that increases in pressure and superficial gas velocity increased the charge for polyethylene resins as measured by a collision probe. Such charge increases would promote particle clustering, which is more dominant for Group A particles than Group B ones. Moughrabiah et al. [84] reported that Group A particles charged significantly more than Group B, and smaller Group B particles charged more than larger Group B ones. The different charging tendencies of different materials lead to different fluidization behavior, and thereby would cause the classification boundaries to shift.

Molerus [62] further proposed that surface hardness may be a secondary factor affecting cohesion. Less elastic particles may be more susceptible to cohesive forces, resulting in Group A particles behaving like Group C. The Group A-B boundary was instead defined with the expression [62]:

$$0.16 \approx \frac{\pi(\rho_p - \rho_f)d_p^3 g}{F_H}$$

where F_H is the inter-particle force, which can be quantified with atomic force microscopy [34]. Fig. 12 illustrates Molerus' [62] criteria on Yang's [19] classification map. It does suggest a more dramatic shift in the A-B boundary than that proposed by Grace [61] or Oltrogge [9], reflecting the significance of inter-particle forces on fluidization behavior.

Royer et al. [34] found that smoother particles were more prone to particle clustering. On a per-mass basis, cluster particles exhibit less drag than singular particles. Such behavior could shift a particle at the Group A-B boundary towards Group B classification.

The understanding of the different interparticle forces and the conditions that dictate them (e.g., adsorbed species [34,36,85], asperities or particle shape [32], etc.) remains incomplete. Nonetheless, the impact of such interactions on the associated fluidization behavior and the Geldart classification is broadly acknowledged.

5.4. Particle shape

Particle sphericity should be considered. Many other correlations for various fluidization-related phenomena, such as terminal velocity [86–89], bed expansion [90], entrainment rates [91], and compaction fraction [92] and Hausner ratio, take sphericity into consideration. Cáceres-Martínez et al. [93] found for biomass fluidization that, along with particle density and particle size, the particle shape had a distinct impact on the fluidization behavior and the fluidization quality. Kruggel-Emden and Vollmari [94] concluded similarly the impact of varying shapes of Group D particles, and proposed revisions to minimum fluidization, slugging, and transitional velocity correlations.

Kunii and Levenspiel indicated that the effective particle diameter is the product of particle sphericity and characteristic particle diameter [23]. Spherical and elongated particles like biomass fluidize significantly differently, specifically with respect to preferential orientations and rotational velocities of particles with different aspect ratios at different parts of the beds and at different superficial gas velocities [95,96]. The non-sphericity of particles is acknowledged to affect flow regime transition [94], drag [97], minimum fluidization velocity [98], bubbling behavior [99], etc. As Guo et al. [100] reported, the irregular plastic particles that were classified as Geldart Group A behaved more like Geldart Group C. As highly non-spherical particles like biomass and plastics become increasingly important in addressing renewable energy and circularity challenges, the effect of sphericity on their classification in the Geldart chart is crucial in providing accurate predictions of the fluidization behaviors.

In terms of the drag forces, less spherical particles have lower terminal velocities. Minimum fluidization velocities and other key velocity metrics are depressed compared to the spherical counterparts. Perhaps

some accountability to particle shape can be addressed in Fig. 12 by using the aerodynamic particle size instead of the pure Sauter-mean particle size. As shown in Fig. 15, this modified Archimedes number provides the expected shift noted by Grace [61] and Oltrogge [9]. However, more data is needed to validate this approach.

For the relatively newer particles of interest like biomass and plastics, not only does the non-sphericity throw the current knowledge base off-kilter, but the low particle density also should be considered. As the Geldart classification chart in Fig. 2 shows, no data point was available for the Geldart B-D demarcation in the lower-density region of <1 g/cm^3, which is the density range of relevance for biomass and plastics. While the current extrapolation can be used as a first pass, some caution is warranted in attempting to predict the fluidization behavior a priori based on the Geldart chart. Indeed, the data-derived boundaries of Grace [61] and Oltrogge [9] further indicate that caution is needed.

6. Concluding remarks

It has been 50 years since the seminal paper on the classification of particles into different fluidization behaviors [1], which persists in remaining the most used grouping in the fluidization community. The classification was described earlier in 1972 [11], but it is the chart presented in 1973 that received widespread use [1]. Specifically, based simply on particle density and particle size, particles are divided into four groups defined as A, B, C and D, which exhibit distinctly different fluidization behaviors. The chart was mainly empirically based on bubbling and aeration behaviors observed during fluidizing by air at ambient conditions, but its application has proliferated beyond such that it is the first question to answer in any design or optimization of processes involving particles. This paper has been cited almost 3000 times, and the number of citations continues to increase, testifying to its relevance to date.

The exalted status of the Geldart classification is not expected to diminish. In particular, computational fluid dynamics – discrete element method (CFD-DEM) (and direct numerical simulation (DNS)) studies, as well as coarse-graining methods [106,107], continue to explore how particles of various sizes behave [85,101–105]. For the larger Geldart Group A, B, and D particles, the results are promising. However, additional validation is needed on how the boundaries between these groups are dependent on elevated temperatures and pressures. As for Geldart Group C and smaller Group A particles, the underlying physics is still under investigation, because of limited understanding of the different interparticle forces and the conditions that dictate them (e.g., adsorbed species [34,36,85], asperities or particle shape [32], etc.). Once resolved, the corresponding refinements of the models would improve predictive capability of the various phenomena in fluidized beds with smaller particles, such as clustering, bubble hydrodynamics, and attrition buffering.

The success of the Geldart classification is testament to simplicity being the ultimate sophistication.

CRediT authorship contribution statement

Ray Cocco: Conceptualization, Methodology, Formal analysis, Investigation, Writing – original draft. **Jia Wei Chew:** Conceptualization, Methodology, Formal analysis, Investigation, Writing – review & editing.

Declaration of Competing Interest

The authors declare that they have no known competing financial interests or personal relationships that could have appeared to influence the work reported in this paper.

Data availability

Data will be made available on request.

References

[1] D. Geldart, Types of gas fluidization, Powder Technol. 7 (1973) 285–292.
[2] D. Geldart, Private Communications, 2006.
[3] M. Baerns, Fluidization of fine particles, in: A.A.H. Drinkenburg (Ed.), Proc. Int. Symp. On Fluidization, Univ. Press, Amsterdam, Eindhoven, Netherlands, 1967, pp. 403–415.
[4] R.A. Brekken, E.B. Lancaster, T.D. Wheelock, Fluidization of flour in a stirred aerated bed: Part I. General fluidization characteristics, Chem. Eng. Prog. Symp. Ser. 66 (1970) 81–90.
[5] J.A.H. De Jong, J.F. Nomden, Homogeneous gas—solid fluidization, Powder Technol. 9 (1974) 91–97.
[6] L. Davies, J.F. Richardson, Trans. Inst. Chem. Eng. 44 (1966) T293–T305.
[7] K. Rietema, Application of mechanical stress theory to fluidization, in: Proc. International Symposium on Fluidization, Eindhoven, 1967, 1967.
[8] K. Godard, J.F. Richardson, Bubble velocities and bed expansions in freely bubbling fluidised beds, Chem. Eng. Sci. 24 (1969) 663–670.
[9] R.D. Oltrogge, Gas Fluidized Bed of Fine Particles, University of Michigan, 1972.
[10] P. Kehoe, J. Davidson, CHEMECA 70, Inst. Chem. Eng. Symp. Ser, Butterworths, Australia, Melbourne 33, 1971, p. 97.
[11] D. Geldart, The effect of particle size and size distribution on the behaviour of gas-fluidised beds, Powder Technol. 6 (1972) 201–215.
[12] K.B. Mathur, Spouted beds (chapter 17), in: J.F. Davidson, D.H. Harrison (Eds.), Fluidization, Academic Press, London and New York, 1971.
[13] R.L. Pigford, T. Baron, Hydrodynamic stability of a fluidized bed, Ind. Eng. Chem. Fundam. 4 (1965) 81–87.
[14] Standard Test Method for Measuring the Minimum Fluidization Velocities of Free Flowing Powders D7742–12, ASTM International West Conshohocken, PA, 2012.
[15] J.P.K. Seville, C.D. Willett, P.C. Knight, Interparticle forces in fluidisation: a review, Powder Technol. 113 (2000) 261–268.
[16] F. Rahman, Fluidization Characteristics of Nanoparticle Agglomerates, Monash University, 2009.
[17] R. Pfeffer, C.H. Nam, R.N. Dave, G. Liu, J.A. Quevedo, Q. Yu, C. Zhu, System and method for nanoparticle and nano-agglomerate fluidization, US Patent, US 7,658,340 B2, 2010.
[18] J.A. Quevedo, R. Pfeffer, In situ measurements of gas fluidized Nanoagglomerates, Ind. Eng. Chem. Res. 49 (2010) 5263–5269.
[19] W.-C. Yang, Modification and re-interpretation of Geldart's classification of powders, Powder Technol. 171 (2007) 69–74.
[20] Y. Zhou, T. Wang, J. Zhu, Investigation on minimum fluidization velocity in a modified Geldart's diagram, Chem. Eng. J. 453 (2023), 139984.
[21] P. Trogadas, V. Ramani, P. Strasser, T.F. Fuller, M.-O. Coppens, Hierarchically structured nanomaterials for electrochemical energy conversion, Angew. Chem. Int. Ed. 55 (2016) 122–148.
[22] J.W. Chew, W.C.Q. LaMarche, R.A. Cocco, 100 years of scaling up fluidized bed and circulating fluidized bed reactors, Powder Technol. 409 (2022), 117813.
[23] D. Kunii, O. Levenspiel, Chapter 3 - fluidization and mapping of regimes, in: D. Kunii, O. Levenspiel (Eds.), Fluidization Engineering, Second edition, Butterworth-Heinemann, Boston, 1991, pp. 61–94.
[24] S.K. Garg, J.W. Pritchett, Dynamics of gas-fluidized beds, J. Appl. Phys. 46 (1975) 4493–4500.
[25] P.U. Foscolo, L.G. Gibilaro, A fully predictive criterion for the transition between particulate and aggregate fluidization, Chem. Eng. Sci. 39 (1984) 1667–1675.
[26] J. Verloop, P.M. Heertjes, Shock waves as a criterion for the transition from homogeneous to heterogeneous fluidization, Chem. Eng. Sci. 25 (1970) 825–832.
[27] N. Menon, D.J. Durian, Particle motions in a gas-fluidized bed of sand, Phys. Rev. Lett. 79 (1997) 3407–3410.
[28] G.D. Cody, D.J. Goldfarb, G.V. Storch, A.N. Norris, Particle granular temperature in gas fluidized beds, Powder Technol. 87 (1996) 211–232.
[29] K. Rietema, The effect of interparticle forces on the expansion of a homogeneous gas-fluidised bed, Chem. Eng. Sci. 28 (1973) 1493–1497.
[30] S.C. Tsinontides, R. Jackson, The mechanics of gas fluidized beds with an interval of stable fluidization, J. Fluid Mech. 255 (1993) 237–274.
[31] J.K. Pandit, X.S. Wang, M.J. Rhodes, Study of Geldart's group a behaviour using the discrete element method simulation, Powder Technol. 160 (2005) 7–14.
[32] J.M. Valverde, A. Castellanos, P. Mills, M.A.S. Quintanilla, Effect of particle size and interparticle force on the fluidization behavior of gas-fluidized beds, Phys. Rev. E 67 (2003), 051305.
[33] J.M. Valverde, M.A.S. Quintanilla, A. Castellanos, P. Mills, Experimental study on the dynamics of gas-fluidized beds, Phys. Rev. E 67 (2003), 016303.
[34] J.R. Royer, D.J. Evans, L. Oyarte, Q. Guo, E. Kapit, M.E. Möbius, S.R. Waitukaitis, H.M. Jaeger, High-speed tracking of rupture and clustering in freely falling granular streams, Nature 459 (2009) 1110–1113.
[35] R. Cocco, F. Shaffer, R. Hays, S.B. Reddy Karri, T. Knowlton, Particle clusters in and above fluidized beds, Powder Technol. 203 (2010) 3–11.
[36] R. Cocco, A. Issangya, S.B.R. Karri, T. Freeman, H.M. Jaeger, T.M. Knowlton, Small-scale particle interactions are having significant effects on global fluidized bed behavior, KONA Powd. Part. J. 34 (2017) 155–167.

[37] Q. Guo, S. Meng, Y. Zhao, L. Ma, D. Wang, M. Ye, W. Yang, Z. Liu, Experimental verification of solid-like and fluid-like states in the homogeneous fluidization regime of Geldart a particles, Ind. Eng. Chem. Res. 57 (2018) 2670–2686.
[38] R. Darton, L. Rd, D. Jf, Bubble growth due to coalescence in fluidized beds, Trans. Inst. Chem. Eng. 55 (1977) 274–280.
[39] H.J. Werther, Der Einfluß des Anströmbodens auf die Strömungsmechanik von Gas/Feststoff-Wirbelschichten, Chemie Ingenieur Technik 49 (1977) 901.
[40] P. Cai, M. Schiavetti, G. De Michele, G.C. Grazzini, M. Miccio, Quantitative estimation of bubble size in PFBC, Powder Technol. 80 (1994) 99–109.
[41] H. Kobayashi, F. Arai, T. Chiba, Behavior of bubbles in a gas-solid fluidized bed, Kagaku-kogaku (Abr. Ed.) 4 (1966) 147–150.
[42] K. Mima, S. Mori, T. Kato, I. Muchi, Behaviour of bubbles in gaseous fluidized beds, Int. Chm. Eng. (1972) 187–194.
[43] D. Geldart, Gas fluidization, in: D. Geldart (Ed.), Gas Fluidization Technology United States, 1986.
[44] M. Pell, Gas fluidization, in: J. Williams, T. Allen (Eds.), Handbook of Powder Technology, Elsevier, 1990.
[45] A. Abrahamsen, D. Geldart, Behaviour of gas-fluidized beds of fine powders Part II. Voidage of the dense phase in bubbling beds, Powder Technol. 26 (1980) 47–55.
[46] R. Cocco, S. Karri, T. Knowlton, Avoid fluidization pitfalls, Chem. Eng. Prog. 110 (2014) 40–45.
[47] A. Issangya, S.R. Karri, T. Knowlton, Why Gas Bypassing Occurs in Deep Fluidized Beds of Geldart Group a Particles and how to Prevent it, Proceedings of the 10th International Conference on Multiphase Flow in Industrial Plant, 2006.
[48] R.A. Cocco, A. Issangya, S.R. Karri, T. Knowlton, Computational Fluid Dynamics of Gas Bypassing in Fluidized Beds with Imposed Solids Flux, the 2008 Annual Meeting, 2008.
[49] D. Geldart, A. Wong, Fluidization of powders showing degrees of cohesiveness—II. Experiments on rates of de-aeration, Chem. Eng. Sci. 40 (1985) 653–661.
[50] S.J. Gelderbloom, D. Gidaspow, R.W. Lyczkowski, CFD simulations of bubbling/collapsing fluidized beds for three Geldart groups, AICHE J. 49 (2003) 844–858.
[51] D. Geldart, A. Wong, Fluidization of powders showing degrees of cohesiveness—I. Bed expansion, Chem. Eng. Sci. 39 (1984) 1481–1488.
[52] D. Geldart, N. Harnby, A. Wong, Fluidization of cohesive powders, Powder Technol. 37 (1984) 25–37.
[53] F. Raganati, R. Chirone, P. Ammendola, Effect of temperature on fluidization of Geldart's group A and C powders: role of interparticle forces, Ind. Eng. Chem. Res. 56 (2017) 12811–12821.
[54] K. Rietema, Powders, what are they? Powder Technol. 37 (1984) 5–23.
[55] D. Song, P. Mehrani, Effect of fluidization pressure on electrostatic charge generation of polyethylene particles, Ind. Eng. Chem. Res. 56 (2017) 14716–14724.
[56] C. Zhu, L.-S. Fan, Dense-Phase Fluidized Beds, Principles of Gas-Solid Flows, Cambridge University Press, Cambridge, 1998, pp. 371–420.
[57] K.B. Mathur, N. Epstein, Dynamics of spouted beds, in: Advances in Chemical Engineering, Elsevier, 1974, pp. 111–191.
[58] N. Epstein, J.R. Grace, Spouted and Spout-Fluid Beds: Fundamentals and Applications, Cambridge University Press, 2010.
[59] O. Gryczka, S. Heinrich, V. Miteva, N.G. Deen, J. Kuipers, M. Jacob, L. Mörl, Characterization of the pneumatic behavior of a novel spouted bed apparatus with two adjustable gas inlets, Chem. Eng. Sci. 63 (2008) 791–814.
[60] S. Yang, L. Zhang, Y. Sun, J.W. Chew, Improving the operational stability of the multi-chamber spout-fluid bed via the insertion of a submerged partition plate, AICHE J. 63 (2017) 485–500.
[61] J.R. Grace, Contacting modes and behaviour classification of gas—solid and other two-phase suspensions, the, Can. J. Chem. Eng. 64 (1986) 353–363.
[62] O. Molerus, Interpretation of Geldart's type A, B, C and D powders by taking into account interparticle cohesion forces, Powder Technol. 33 (1982) 81–87.
[63] W.R.A. Goossens, Classification of fluidized particles by Archimedes number, Powder Technol. 98 (1998) 48–53.
[64] S. Ergun, Fluid flow through packed columns, Chem. Eng. Prog. 48 (1952) 89–94.
[65] O. Molerus, Principles of Flow in Disperse Systems, Chapman & Hall, London, 1993.
[66] H. Kalman, A. Satran, D. Meir, E. Rabinovich, Pickup (critical) velocity of particles, Powder Technol. 160 (2005) 103–113.
[67] J.S. Halow, Incipient rolling, sliding and suspension of particles in horizontal and inclined turbulent flow, Chem. Eng. Sci. 28 (1973) 1–12.
[68] A. Anantharaman, J.R. van Ommen, J.W. Chew, Minimum pickup velocity (Upu) of nanoparticles in gas–solid pneumatic conveying, J. Nanopart. Res. 17 (2015) 470.
[69] F.J. Cabrejos, G.E. Klinzing, Minimum conveying velocity in horizontal pneumatic transport and the pickup and saltation mechanisms of solid particles, Bulk Solids Handl. 14 (1994) 541–550.
[70] F.J. Cabrejos, G.E. Klinzing, Pickup and saltation mechanisms of solid particles in horizontal pneumatic transport, Powder Technol. 79 (1994) 173–186.
[71] F.J. Cabrejos, G.E. Klinzing, Incipient motion of solid particles in horizontal pneumatic conveying, Powder Technol. 72 (1992) 51–61.
[72] K.S. Hayden, K. Park, J.S. Curtis, Effect of particle characteristics on particle pickup velocity, Powder Technol. 131 (2003) 7–14.
[73] V.K. Gupta, G. Shanker, N.K. Sharma, Experiment on fluid drag and viscosity with an oscillating sphere, Am. J. Phys. 54 (1986) 619–622.
[74] R. Cocco, S. Karri, T. Knowlton, Introduction to fluidization, Chem. Eng. Prog. (2014) 21–29.
[75] D. Liu, M. Kwauk, H. Li, Aggregative and particulate fluidization—the two extremes of a continuous spectrum, Chem. Eng. Sci. 51 (1996) 4045–4063.
[76] M. Rhodes, Chapter 1 Particle Size Analysis, Introduction to Particle Technology, 2008, pp. 1–28.
[77] A.K. Marnani, A. Bück, S. Antonyuk, B. van Wachem, D. Thévenin, J. Tomas, The effect of the presence of very cohesive Geldart C ultra-fine particles on the fluidization of Geldart A fine particle beds, Processes 7 (2019) 35.
[78] A.S. Issangya, S.B. Reddy Karri, T. Knowlton, R. Cocco, Use of pressure to mitigate gas bypassing in fluidized beds of FCC catalyst particles, Powder Technol. 290 (2016) 53–61.
[79] P. Bareschino, T. Gravina, L. Lirer, A. Marzocchella, P. Petrosino, P. Salatino, Fluidization and de-aeration of pyroclastic mixtures: the influence of fines content, polydispersity and shear flow, J. Volcanol. Geotherm. Res. 164 (2007) 284–292.
[80] T. Yehuda, H. Kalman, Geldart classification for wet particles, Powder Technol. 362 (2020) 288–300.
[81] J.P.K. Seville, R. Clift, The effect of thin liquid layers on fluidisation characteristics, Powder Technol. 37 (1984) 117–129.
[82] F. Fotovat, X.T. Bi, J.R. Grace, Electrostatics in gas-solid fluidized beds: a review, Chem. Eng. Sci. 173 (2017) 303–334.
[83] P. Mehrani, M. Murtomaa, D.J. Lacks, An overview of advances in understanding electrostatic charge buildup in gas-solid fluidized beds, J. Electrost. 87 (2017) 64–78.
[84] W.O. Moughrabiah, J.R. Grace, X.T. Bi, Electrostatics in gas–solid fluidized beds for different particle properties, Chem. Eng. Sci. 75 (2012) 198–208.
[85] H.Y. Xie, The role of interparticle forces in the fluidization of fine particles, Powder Technol. 94 (1997) 99–108.
[86] A. Haider, O. Levenspiel, Drag coefficient and terminal velocity of spherical and nonspherical particles, Powder Technol. 58 (1989) 63–70.
[87] C. Zhou, J. Su, H. Chen, Z. Shi, Terminal velocity and drag coefficient models for disc-shaped particles based on the imaging experiment, Powder Technol. 398 (2022), 117062.
[88] F. Dioguardi, D. Mele, A new shape dependent drag correlation formula for non-spherical rough particles. Experiments and results, Powder Technol. 277 (2015) 222–230.
[89] M. Hartman, O. Trnka, K. Svoboda, Free settling of nonspherical particles, Ind. Eng. Chem. Res. 33 (1994) 1979–1983.
[90] V.J. Inglezakis, M. Stylianou, M. Loizidou, Hydrodynamic studies on zeolite fluidized beds, Int. J. Chem. React. Eng. 8 (2010).
[91] W. de Vos, W. Nicol, E. du Toit, Entrainment behaviour of high-density Geldart a powders with different shapes, Powder Technol. 190 (2009) 297–303.
[92] K. Tannous, P.S. Lam, S. Sokhansanj, J.R. Grace, Physical properties for flow characterization of ground biomass from Douglas fir wood, Part. Sci. Technol. 31 (2013) 291–300.
[93] L.E. Cáceres-Martínez, D.C. Guío-Pérez, S.L. Rincón-Prat, Significance of the particle physical properties and the Geldart group in the use of correlations for the prediction of minimum fluidization velocity of biomass–sand binary mixtures, Biomass Conv. Biorefin. 13 (2023) 935–951.
[94] H. Kruggel-Emden, K. Vollmari, Flow-regime transitions in fluidized beds of non-spherical particles, Particuology 29 (2016) 1–15.
[95] I. Mema, K.A. Buist, J.A.M. Kuipers, J.T. Padding, Fluidization of spherical versus elongated particles: experimental investigation using magnetic particle tracking, AICHE J. 66 (2020), e16895.
[96] C. Li, X. Gao, S.L. Rowan, B. Hughes, W.A. Rogers, Measuring binary fluidization of nonspherical and spherical particles using machine learning aided image processing, AICHE J. 68 (2022), e17693.
[97] L. Lu, X. Gao, M. Shahnam, W.A. Rogers, Coarse grained computational fluid dynamic simulation of sands and biomass fluidization with a hybrid drag, AICHE J. 66 (2020), e16867.
[98] A. Reyes-Urrutia, J. Soria, A. Saffe, M. Zambon, M. Echegaray, S.G. Suárez, R. Rodriguez, G. Mazza, Fluidization of biomass: a correlation to assess the minimum fluidization velocity considering the influence of the sphericity factor, Part. Sci. Technol. 39 (2021) 1020–1040.
[99] D. Bannon, M. Deza, M. Masoumi, B. Estejab, Assessment of irregular biomass particles fluidization in bubbling fluidized beds, Energies 16 (2022) 2051.
[100] Q. Guo, Y. Liu, M. Wang, Fluidization characteristics of printed circuit board plastic particles with different sizes, the, Can. J. Chem. Eng. 88 (2010) 710–717.
[101] H.P. Zhu, Z.Y. Zhou, R.Y. Yang, A.B. Yu, Discrete particle simulation of particulate systems: a review of major applications and findings, Chem. Eng. Sci. 63 (2008) 5728–5770.
[102] J. Wang, A review of Eulerian simulation of Geldart a particles in gas-fluidized beds, Ind. Eng. Chem. Res. 48 (2009) 5567–5577.
[103] A. Gómez-Barea, B. Leckner, Modeling of biomass gasification in fluidized bed, Prog. Energy Combust. Sci. 36 (2010) 444–509.
[104] C. Loha, S. Gu, J. De Wilde, P. Mahanta, P.K. Chatterjee, Advances in mathematical modeling of fluidized bed gasification, Renew. Sust. Energ. Rev. 40 (2014) 688–715.
[105] N.G. Deen, E.A.J.F. Peters, J.T. Padding, J.A.M. Kuipers, Review of direct numerical simulation of fluid–particle mass, momentum and heat transfer in dense gas–solid flows, Chem. Eng. Sci. 116 (2014) 710–724.
[106] A. Di Renzo, E.S. Napolitano, F.P. Di Maio, Coarse-grain DEM modelling in fluidized bed simulation: a review, Processes 9 (2021) 279.
[107] J. Wang, Continuum theory for dense gas-solid flow: a state-of-the-art review, Chem. Eng. Sci. 215 (2020), 115428.